Coastal Engineering 199 (2025) 104742

Contents lists available at ScienceDirect

Coastal Engineering

journal homepage: www.elsevier.com/locate/coastaleng

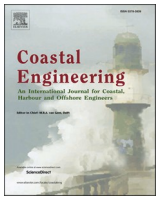

Designing modular, artificial reefs for both coastal defense and coral restoration

Benjamin K. Norris [a,*], Borja G. Reguero [a,b], Joseph Bartolai [c], Michael A. Yukish [d], Landolf Rhode-Barbarigos [e], Brian K. Haus [f], Gabriel Barajas Ojeda [g], Maria Maza [g], Javier L. Lara [g], Michael W. Beck [a]

[a] Institute of Marine Sciences and Center for Coastal Climate Resilience, University of California, Santa Cruz, 115 McAllister Way, Santa Cruz CA 95060, USA
[b] Coastal Science and Policy, University of California, Santa Cruz, 115 McAllister Way, Santa Cruz CA 95060, USA
[c] Applied Research Laboratory, The Pennsylvania State University, University Park 16803 PA, USA
[d] Department of Aerospace Engineering, The Pennsylvania State University, University Park 16803 PA, USA
[e] Department of Civil and Architectural Engineering, College of Engineering, University of Miami, 1251 Memorial Drive McArthur, Coral Gables, FL 33146, USA
[f] Department of Ocean Sciences, Rosenstiel School of Marine, Atmospheric, and Earth Science, University of Miami, 4600 Rickenbacker Causeway, Miami, FL 33149-1031, USA
[g] Instituto de Hidráulica Ambiental de la Universidad de Cantabria (IHCantabria), Isabel Torres 15, 39011, Santander, Spain

ARTICLE INFO

Keywords:
Artificial reefs
Coastal structures
Wave transformation
Computational fluid dynamics
OpenFOAM
Coral reef restoration

ABSTRACT

Coastal flooding and erosion are growing issues for coastal communities as their severity continues to worsen with climate change. As a result, there is increasing interest in the use of nature-based engineering as a sustainable and cost-effective strategy for protecting many coastlines globally. Among these approaches, reef engineering aims to integrate both the physical and biological aspects of reef communities to attenuate incident wave energy while still maintaining ecological values. However, few examples currently exist on reef engineering for coastal defense due to the multidisciplinary challenge of constraining physical and biological interactions with artificial reefs. Here, we present the first design iteration of a novel artificial hybrid reef system that intends to provide both coastal defense benefits as well as refugia for corals to enable their future growth. To balance these performance objectives, the pyramidal low-crested reef designs developed here combine two hexagonal sub-units: SEAHIVE® and lattice with tunable porosity. The hydrodynamic performance of these sub-units was tested using a numerical wave tank (NWT), based on the computational fluid dynamics (CFD) modeling suite OpenFOAM, to determine the best configuration of the sub-units for a given set of wave conditions, both as single reefs and as a three-row reef system. The goal was to produce a small subset of reef designs to be tested in a wave flume facility to support model calibration and future design iteration. The reef designs explored herein offer wave energy reduction values greater than 70%, consistent with natural coral reefs as well as other conventional submerged breakwater designs. Further, the highly porous sub-units provide further tunability of hydrodynamic performance when compared with traditional low-crested breakwaters.

1. Introduction

Coastal flooding and erosion due to extreme weather events annually affects thousands of vulnerable coastal communities globally, and such hazards are predicted to worsen during this century due to population growth and sea level rise (Barnard et al., 2019; Vitousek et al., 2017). The need for marine infrastructure will likely escalate as demands for defenses of ports, harbors, and coastal cities increases with rising sea levels and the intensity of storms and flooding (Asif and Muneer, 2007). Much like fringing natural coral reef crests, engineered low-crested structures are designed to enhance wave breaking atop the structure, thereby decreasing wave heights and associated hazards such as flooding and erosion at shore (Beck and Lange, 2016; Rogers et al., 2013; Sheppard et al., 2005). Conventional structures such as submerged rubble-mound 'reef' breakwaters are widely applied as a solution for coastal defense. However, these structures may damage existing ecosystems by disrupting biological connectivity or concentrating wave energy in a particular area (Cooper and Pilker, 2012; Dafforn et al.,

* Corresponding author.
E-mail address: bknorris@ucsc.edu (B.K. Norris).

https://doi.org/10.1016/j.coastaleng.2025.104742
Received 13 November 2024; Received in revised form 3 March 2025; Accepted 4 March 2025
Available online 4 March 2025

2015; Moschella et al., 2005). To mitigate these effects and increase habitat benefits, engineered coastal structures should mimic natural (porous) reefs to allow water to circulate within, thereby enhancing wave energy reduction and at the same time, creating refugia for biological communities. Artificial-biological hybrid reef designs (hereafter, 'hybrid reefs') may perform a similar function as traditional structures with respect to coastal defense, yet they differ in that they are intended to provide greater ecological benefit than traditional rubble-mount breakwaters (Storlazzi et al., 2025). These co-benefits may emerge from the use of biophilic concrete mixtures (to enhance biological productivity at the surface of the structure) that is cast or 3D printed into complex shapes to mimic the structural complexity of natural reefs (Diederen, 2022; van den Brekel, 2021). Hence, hybrid reefs must optimize the material, geometry, inner structural complexity, and placement relative to shore, to provide both coastal defense and ecological benefits (Reguero et al., 2018; Viehman et al., 2023).

Healthy, natural coral reefs are an effective offshore barrier and can reduce most wave energy that would otherwise impact the shoreline (Lowe et al., 2005; Monismith et al., 2015; Pequignet et al., 2011; Rogers et al., 2015). The coastal protection services offered by coral reefs are therefore greater than many other marine ecosystems (Ferrario et al., 2014). In the United States, coral reefs were valued for their role in coastal flood mitigation at over $1.8 billion (Reguero et al., 2021) leading to their designation as national natural infrastructure (USCRTF, 2020). As such, The Reef Engineering to Enhance Future Structures (X-REEFS) project was funded by the United States Defense Advanced Research Projects Agency (DARPA) to develop a hybrid artificial-biological reef system to mitigate coastal hazards in coralline environments, now and in the future.

The present work adds to a growing corpus of artificial reef designs that intend to provide habitat for reef-forming organisms, such as Reef Ball, Reefy, and ReefSystems (Barber and Krumholz, 2007; Diederen, 2022; van den Brekel, 2021). Unlike these existing designs, the novel lattices explored here can redirect water flow through specific, engineered pathways, reducing wave transmission across the structure. The combination of these lattices and the existing SEAHIVE® design (Rhode-Barbarigos, 2022) are intended to provide a flexible solution for coastal hazard risk management while providing additional habitat creation benefits. Such artificial reef designs may be employed in locations where coral reefs have become degraded to the point that they no longer provide coastal defense benefits, or in locations where corals could grow but lack the appropriate substrate on which to colonize. In general, one of the key challenges in designing artificial reefs is a lack of direct comparisons due to the wide variety of approaches, design choices, and intended coastal settings. As much work already exists in the optimization of traditional breakwaters, these provide a framework for assessing the new reef designs.

In general, the wave dissipation capabilities of a breakwater or low-crested structure (LCS) is often characterized by the wave transmission coefficient K_t [−], defined as the ratio between the incoming and transmitted wave height, or how incoming wave heights are reduced across the structure (Goda and Ahrens, 2009; Seelig, 1980). K_t is influenced by both wave interactions across and around the structure, as well as water interactions within the structure. Reef-type structures are a special type of LCS that can be reshaped by wave attack (van der Meer and Pilarczyk, 1990). They are dynamically stable and are made of homogeneous material (stones) without a filter layer or core (Ahrens, 1984). These 'reef breakwaters' may also initially be designed as an emergent structure and after reshaping become a submerged structure. Substantial experimentation has demonstrated that LCS performance varies strongly with the relative freeboard R_c/H_i [−], with the structure freeboard R_c [m] and the incident wave height before the structure H_i [m] (van der Meer and Pilarczyk, 1990). Furthermore, LCS presents an economic advantage over emergent breakwaters due to a reduction in the cost of construction, as costs scale with the height of the crest (Sharifahmadian, 2015).

However, unlike traditional LCS designs, artificial 'hybrid' reefs are typically composed of only a few repeating units to create the bulk of the structure (for examples, see: Diederen (2022); Mendoza et al. (2019); Woo et al. (2014)). Such units have tunable parameters that include the porosity and transmissivity of water flow through the structure. Wave flume studies have shown that such highly permeable structures present similar behavior to impermeable rubble-mound LCS with similar K_t values when the internal structure is optimized to disrupt wave orbital motions (Van Gent et al., 2023). However, most LCS and reef breakwaters designs to date, and hence engineering formulations, reflect singular trapezoidal shapes with either emergent ($R_c > 0$) or submerged ($R_c < 0$) crests made of concrete or rock rubble. Although fewer empirical relationships exist for hybrid reefs, recent work by van den Brekel (2021) and Van Gent et al. (2023) suggests that K_t can largely be described by R_c/H_i, with the greatest reduction in wave transmission occurring with a complex, three-dimensional (3D) hybrid reef structure with shallow freeboard. Similarly, Vijay et al. (2021) indicates that wave transmission for multi-row hybrid reef structures scales with the number of reef units, with better performance (lower K_t) achieved with three or more rows. We follow this guidance for the hybrid reef development considered here.

The purpose of this study is to design highly porous artificial reef structures that enhance internal energy dissipation and thus reduce wave transmission across the reef. The intention is to create a designed and effective wave break that can also provide refugia for benthic organisms. Here, we compare different novel hybrid reef concepts, comprised of individual sub-units (SEAHIVE, lattice) and arranged in shore-parallel rows, in terms of wave energy reduction and flow through the structures. Performance testing was accomplished using a computational fluid dynamics (CFD) tool to assess the reefs' hydrodynamic properties. As the goal of this work was to develop prototype reef designs for eventual wave flume testing, the CFD tool enabled relatively rapid performance testing across a wide range of reef designs and wave conditions without the need for physically constructing all the reef units. In the following section, we describe the numerical model setup, data analysis methodologies, and experimental design. Section 3 presents the results of the CFD tests, and Section 4 comparisons with literature values. The conclusions of the study and recommendations for future work are presented in Section 5.

2. Methods

This study details a series of 3D CFD models that were run, first on single-row reefs, and then on multi-row reefs, to assess the hydrodynamic performance of the reef units in terms of standard metrics for assessing low-crested structures: the wave transmission coefficient K_t, the wave reflection coefficient K_r, and the wave energy reduction coefficient $1 - K_t^2$. The 3D models were critical for assessing the different porosities of each reef design as well as flow within and above the reef structures in response to wave forcing. Prior to the 3D modeling, a sensitivity analysis was performed to determine design criteria like the number of reef rows, the reef freeboard, and the spacing between reef rows. In the following sections, the individual sub-units are first described, then the model set-up and configuration are detailed, followed by a description of the model scenarios that were run to assess each reef configuration, and finally the model data analysis and performance metrics.

2.1. Reef structure sub-unit definition

The hybrid artificial reefs considered here are composed of two different hexagonal sub-units: the SEAHIVE® system (Fig. 1a and b) and a novel gyroid lattice (Fig. 1c) that was designed to be compatible with the hexagonal SEAHIVE system. The reefs, therefore, can be composed of different combinations of these elements to create different flow

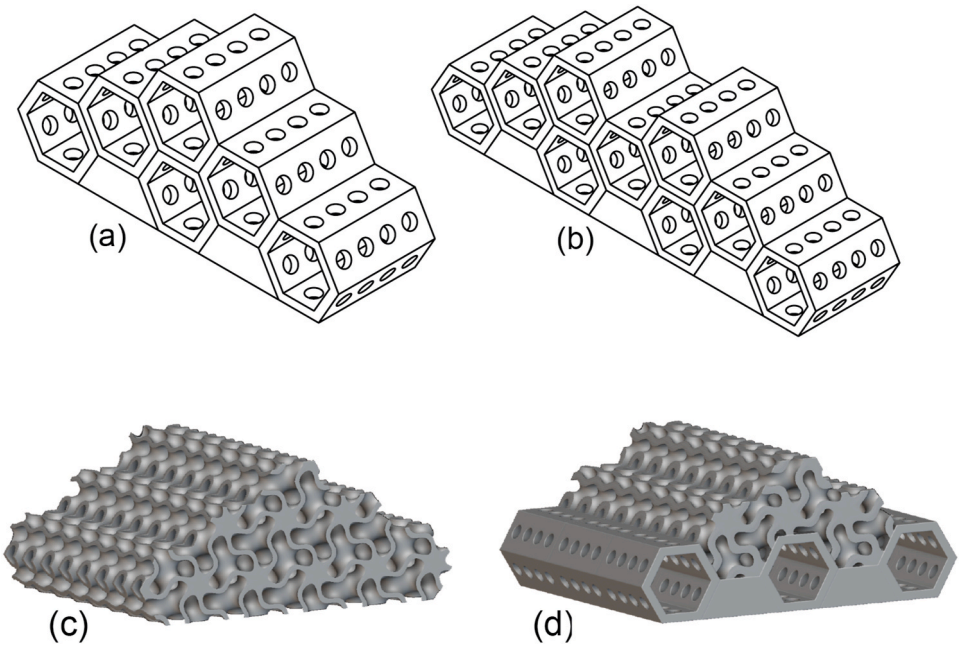

Fig. 1. Pyramidal, highly porous artificial reef designs tested in this study. (a–b) two variants of the SEAHIVE system consisting of stacks of 6 (a) and 9 (b) perforated hexagonal sub-units (shorthand: 6-unit and 9-unit, respectively). (c) a gyroid equation-based lattice breakwater with 30% volume fraction with the same external dimensions as the 6-unit SEAHIVE reef. (d) an example combined 6-unit reef, demonstrating one possibility for integrating the two sub-unit systems. In this example, the lattice uses a 55% volume fraction.

properties. A numerical wave tank (NWT), based on CFD modeling, was developed to assess the flow properties of each design in isolation, and then as a two-part system (Fig. 1d), to determine the strengths of both systems and to optimize wave attenuation performance and internal energy dissipation.

2.1.1. SEAHIVE sub-units

SEAHIVE is a marine and estuarine shoreline protection system based on hexagonal perforated prisms (Ghiasian et al., 2019a, 2019b). Perforations on the side faces of the hexagonal units form interconnected channels resulting in a honeycomb-like structure that is designed to allow water to circulate within the structure, dissipating wave energy through turbulence, and reducing wave transmission. The faceted perforated geometry of the SEAHIVE system also increases the complexity of the structure which, when combined with the use of an ecofriendly material such as a biophilic concrete mixture with non-corrosive reinforcement, is expected to increase the system's potential for habitat creation (Pioch and Souche, 2021). Although different SEAHIVE designs exist, in this study, a variant of the system with hexagonal faces measuring 1.5 m in corner-to-corner distance was arranged in pyramidal stacks of 6- and 9-hexagonal sub-units (hereafter, 6- and 9-units; Fig. 1a and b) with respective fixed porosity of 0.625 and 0.560.

2.1.2. Lattice sub-units

The second sub-unit type is a hexagonal gyroid lattice, which was designed to integrate with the SEAHIVE sub-units and provide adjustable water velocity dampening, based on the composition of the lattice structure. The gyroid unit (Fig. 2) consists of an equation-based lattice that provides a porous structure with high tortuosity that channels water in a helical path through the structure, enhancing frictional dissipation and potentially providing refugia for marine life. This flow pathway can be explicitly engineered by varying the geometric parameters of the lattice.

The gyriod Triply Periodic Minimal Surface (TPMS) (Fig. 2a) can be approximated using a Fourier series combination of trigonometric functions (Eq. (1); von Schnering and Nesper, 1991):

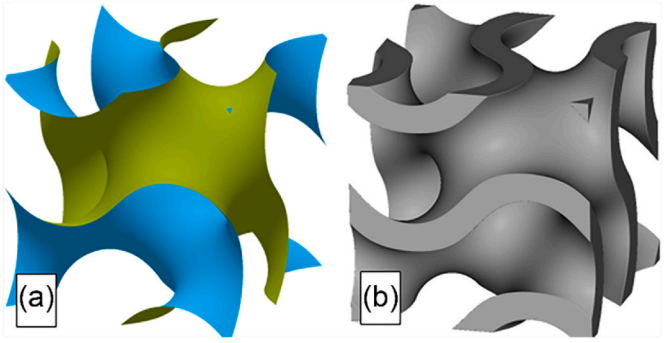

Fig. 2. A single unit cell of both the gyroid Triply Periodic Minimal Surface (TPMS) (a) and the gyroid equation-based lattice (b).

$$\sin\left(\frac{2\pi}{P}x\right)\cos\left(\frac{2\pi}{P}y\right)+\sin\left(\frac{2\pi}{P}y\right)\cos\left(\frac{2\pi}{P}z\right)+\sin\left(\frac{2\pi}{P}z\right)\cos\left(\frac{2\pi}{P}x\right)=0 \tag{1}$$

Where (x,y,z) is a location in $\mathbb{R}^3$ and P is the period of the function in $\mathbb{R}^3$. The set of points within $\mathbb{R}^3$ that satisfy this equation will approximate the gyroid TPMS. Like the TPMS, this approximation is infinitely thin and therefore not particularly useful for coastal engineers. However, the gyroid equation can be modified to produce a lattice structure with the addition of a thickness parameter (t) and changing the equation to an inequality (Eq. (2); Fisher et al., 2023):

$$\left|\sin\left(\frac{2\pi}{P}x\right)cos\left(\frac{2\pi}{P}y\right)+\sin\left(\frac{2\pi}{P}y\right)\cos\left(\frac{2\pi}{P}z\right)+\sin\left(\frac{2\pi}{P}z\right)\cos\left(\frac{2\pi}{P}x\right)\right|\leq t \tag{2}$$

This form of the equation will provide a gyroid equation-based lattice structure (Fig. 2b) that can be cast or 3D-printed in concrete to be used in coastal engineering purposes as an element of a hybrid reef breakwater. The volume fraction (VF) of the lattice structure can be adjusted and optimized for flow conditions by changing the parameter t

in Eq. (2), but it should be noted that the physical wall thickness of the equation-based lattice structure is dependent on both the thickness parameter and period of the equation. Here, the lattice geometry was generated in nTop (nTopology Inc., New York, NY USA) utilizing Eq. (2) and varying t to generate wall thicknesses corresponding to VF of 25%–55% at steps of 5%. Each of these lattice designs were tested with the NWT (Section 3) to determine the optimal VF to attenuate incident waves.

2.2. Numerical model description

In this study, numerical simulations were conducted in the open-source CFD model OpenFOAM (version-2206). In the models, the *interFoam* solver was used to iteratively solve the Reynolds-Averaged Navier Stokes (RANS) equations that encompass the conservation of mass and momentum of fluid flow for two incompressible phases (air and water) using a Volume of Fluid (VoF) approach. These equations are represented as follows:

$$\frac{\partial u_i}{\partial x_i} = 0 \tag{3}$$

$$\frac{\partial \rho u_i}{\partial t} + u_j \frac{\partial \rho u_i}{\partial x_j} = -\frac{\partial p^*}{\partial x_i} + g_j x_j \frac{\partial \rho}{\partial x_i} + f_{\sigma i} + \frac{\partial}{\partial x_j} \mu_{eff} \left(\frac{\partial \rho u_i}{\partial x_j} + \frac{\partial \rho u_j}{\partial x_i} \right) \tag{4}$$

$$\frac{\partial \alpha}{\partial t} + \frac{\partial u_i \alpha}{\partial x_i} + \frac{\partial u_{ci} \alpha (1-\alpha)}{\partial x_i} = 0 \tag{5}$$

where u_i [m/s] are the ensemble averaged components of the velocity, x_i [m] the Cartesian coordinates, g_j [m/s^2] the components of the gravitational acceleration, ρ [kg/m^3] the density of the fluid, p^* [Pa] the ensemble averaged pressure in excess of hydrostatic, α [−] the volume fraction (VoF), $f_{\sigma i}$ [N/m^3] the surface tension, u_{ci} is the compression velocity [m/s], μ_{eff} [Pa•s] is the effective dynamic viscosity that is defined as $\mu_{\text{eff}} = \mu + \rho\nu_t$ and takes into account the dynamic molecular (μ) and the turbulent viscosity effects ($\rho\nu_t$). The VoF method (Hirt and Nichols, 1981) represents the air phase as $\alpha = 0$, the water phase as $\alpha = 1$.

Since pressure and velocity are coupled, the solution to both fields are obtained using a two-step approach. We employed the PIMPLE algorithm built-in to OpenFOAM to iteratively solve the continuity and momentum equations and the MULES algorithm to solve the VoF equation. Turbulence closure was solved with the $k - \omega$ *SST* model (Menter, 1994), as it combines the advantages of the original $k - \omega$ model (Wilcox, 2006) for boundary layer effects near walls (impermeable objects in the model domain) and the $k - \varepsilon$ model (Jones and Launder, 1973) away from walls. In this study, the $k - \omega$ *SST* turbulence model was employed and enhanced as per Larsen and Fuhrman (2018) to limit turbulence overproduction beneath surface waves. The reader is referred to Larsen and Fuhrman (2018) for further reading on the stabilized turbulence models.

Waves were simulated using the IHFOAM toolbox for *interFoam* (Higuera et al., 2013, 2014). Although other alternatives exist (Jacobsen et al., 2012), the IHFOAM toolbox is advantageous because it is included in the OpenFOAM distribution, is robust and computationally efficient (e.g., Vyzikas et al., 2018), and has been extensively validated for coastal engineering applications (Di Paolo et al., 2021; Higuera et al., 2014; Maza et al., 2015).

2.3. Numerical wave tank

Experiments were conducted at a 1:5 model to prototype scale. An NWT 22 m in length, 1 m in width, and 4 m in height was developed to accommodate a constant water depth of $h = 0.6$ m (3.0 m at prototype scale) and the range of wave heights used in experimentation. Experimental wave conditions (Section 2.4) were scaled by matching the Froude number to ensure the correct scaling of gravity forces to yield a space-scaling factor of 1:5 and a time-scaling factor of $1 : \sqrt{5}$. Reef units extended across the entire width of the model to avoid edge effects in the spanwise dimension.

To generate the final domains, 3D STL (stereolithography file) models of the reef structures were placed inside the model domains and were 'snapped' to the bottom of the model domains using the *snappyHexMesh* utility in OpenFOAM. Grid-cell independence was determined by running a series of empty wave tank models with turbulence and with increasing grid resolution for each set of wave conditions to determine the resolution at which (i) wave heights did not decay with distance along the x-axis of the wave flume, and (ii) space-averaged water velocity profiles converged. This process produced a grid resolution that balanced both precision and computational cost. Hence, all domains used an initial grid resolution of $\Delta x = \Delta y = \Delta z = 0.04$ m for the in-water region of the domain. Model grids were refined down to $\Delta x = 0.02$ m in the region containing the free surface, and $\Delta x = 0.01$ m near the bottom wall and the reef structures (Fig. 3). Such mesh refinement enabled the resolution of the holes in the geometry to allow flow through the reef structures. For the in-air region of the domain, cells were stretched in the vertical dimension (Δz) to slightly reduce computational costs. The resultant meshes ranged between 3.4 and 5.6 million cells.

All models employed the following boundary conditions. For the velocity field, the model inlet and outlet used the *waveVelocity* boundary condition for wave generation and absorption, respectively. The bottom wall and reef structures employed a uniform *fixedValue* of (0 0 0) as an initialization, the side walls employed the *slip* boundary condition to minimize wall effects in a relatively narrow domain, and the top (atmosphere) used the *pressureInletOutletVelocity* condition. For the pressure field, the *fixedFluxPressure* condition was applied to adjust the pressure gradient so that the boundary flux matched the velocity boundary condition for all walls except the atmosphere, which employed the *totalPressure* condition. Wave generation (*cnoidal* theory) and active absorption (*shallowWaterAbsorption*) were used at the inlet and outlet boundaries to reduce wave reflections inside the model domain.

Wall functions were used to model boundary layer flow in the near-wall regions without resolving the boundary layer. Time-averaged values of the dimensionless wall distance $z+$ ranged from 30 to 150, were $30 < z+ < 300$ defines the log-layer where wall functions are applicable. Initial values of the turbulence fields (*k*, *omega, nut*) were set using standard equations with $C_\mu = 0.09$, turbulent intensity of 5%, depth-averaged velocity from the empty wave tank models, and turbulent length scale set by the freeboard (R_c) above the reef structures. These initialization conditions do not affect the wave solution, as wave-structure interaction is a highly turbulent process, and turbulence production and dissipation are largely controlled by the acceleration and rotation of fluid flow around, within, and above the reef structure(s).

2.4. Model scenario and NWT test development

Before any CFD modeling was conducted, a scaling analysis based on the empirical equations of Tomasicchio and D'Alessandro (2013) was performed to estimate K_t and K_r for n rows of identical, solid reef units for a constant water depth of $h = 0.6$ m (3.0 m prototype scale) and wave heights of $H = 0.2$–0.4 m (1.0–2.0 m) with periods $T = 3.57$–6.26 s (8.0–14.0 s). For simplicity, the reef structures were assumed to be impermeable with a bottom and crest width equivalent to the 6-unit SEAHIVE design (Fig. 1a), and a range of $n = 1$ to 6 rows of identical reefs. This analysis suggested that K_t decreased with the number of reefs and wave height, and increased with wave period. Furthermore, the scaling analysis indicated that multiple rows ($n > 2$) would be necessary to produce sufficient wave height reduction.

Second, a series of 2D OpenFOAM simulations were conducted to determine both the optimal freeboard and row spacing (S) between

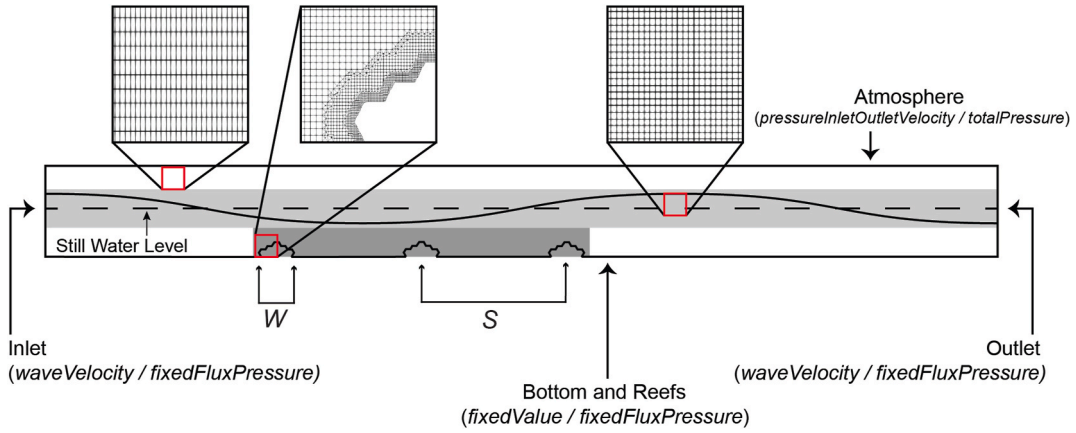

Fig. 3. Example of model domain from OpenFOAM showing varying degrees of mesh refinement. Boundary conditions for the velocity and pressure fields at the inlet, outlet, bottom, and atmosphere are denoted with arrows in these respective areas. The side walls (not shown) used the *slip* boundary condition for the velocity and turbulence fields. The definitions of W, the reef-unit-width and S, the reef row spacing, defined as the center-to-center distance between adjacent reef rows, are as indicated.

adjacent reefs. For these scenarios, the NWT was 22 m long, 0.01 m wide, and 4 m high, thus reducing the computational costs by not resolving fluid flow in the spanwise direction. All boundary conditions were kept the same as the 3D NWT, except for the front and back patches, which were defined as *empty* (non-computational) in OpenFOAM. In these simulations, the water depth was kept constant at $h = 0.6$ m (3.0 m), and monochromatic waves with heights of $H = 0.2$, 0.3, and 0.4 m (1.0–2.0 m) and periods of $T = 3.57$, 4.47, and 5.37 s (8.0–12.0 s) were used to assess the performance of each reef design. Impermeable (solid) versions of both the 6- and 9-unit SEAHIVE reefs with sub-unit diameters of 0.9, 1.2, and 1.5 m were simulated, resulting in freeboards ranging in $R_c = -0.35$, -0.12, and -0.08 m for the 0.9, 1.2, and 1.5 m sub-unit diameter reefs, respectively. Rows of $n = 1$ to 4 reefs were considered for each reef type (6- or 9-unit) and sub-unit diameter, and the row spacing S varied from $1W$ to $4W$, where S is the center-to-center spacing between adjacent reefs, and W is the reef width (Fig. 3). Through this exercise, it was determined that a reef layout consisting of either 6-unit or 9-unit reefs had the best performance (lowest K_t) with the shallowest freeboard ($R_c = -0.08$), $n = 3$ rows, and row spacing $S = 3W$ [not shown for brevity]. Such a design caused the incident waves to break across the first reef, due to the shallow freeboard, thereby enhancing the wave energy reduction across the total reef structure. These design parameters were carried into the 3D modeling.

The porous SEAHIVE, lattice, and hybrid SEAHIVE-lattice reef designs (Fig. 1) were simulated in 3D NWT with OpenFOAM to resolve the interaction between external and internal flows. We considered four different test cases (Table 1): single-row SEAHIVE 6- and 9-unit reefs, single-row 6-unit lattice reefs, and three-row hybrid SEAHIVE-lattice reefs with row spacing set to $S = 3W$ (for some examples, please see Supplementary Materials). The single-row SEAHIVE reefs were named according to their number of hex sub-units (i.e., 9-unit and 6-unit); the lattice reefs used the 6-unit configuration and were characterized by their volume fraction (VF) as a percentage (e.g., 25%, 35%, 45%, etc.). The three-row SEAHIVE and hybrid reefs used the following naming convention: for SEAHIVE-only designs, these were designated 'SEAHIVE-3row'. For hybrids of SEAHIVE and lattice, these were designated 'Hybrid-3row-*N*', where N is a unique integer relating to a particular configuration ranging from 1 to 26. These configurations are described in greater detail in Section 3.3. Each configuration was run once per wave condition listed in Table 1.

For all models, wave trains of 30 monochromatic waves were generated, with data analysis being performed on the last 15 waves, after a quasi-steady state was established inside the models. The initial SEAHIVE reef models were run with model-scale wave heights ranging from $H = 0.2$–0.4 m (1.0–2.0 m prototype scale) and periods ranging from $T = 3.57$–5.37 s (8.0–12.0 s) to capture the range of common wave conditions in an offshore environment with a mean water depth of $h =$

Table 1
Optimization tests completed with the three-dimensional NWT for a range of novel reef designs: SEAHIVE, lattice, and a hybrid combination of SEAHIVE and lattice. Here, h is the water depth [m], R_c is the freeboard [m], H the wave height [m], T the wave period [s], n the number of rows of reefs [−], and S the center-to-center spacing between adjacent rows in reef-widths [−]. All tests were conducted at 1:5 physical scale and 1: $\sqrt{5}$ time scale. The average reef porosity was calculated using the volumetric estimator in Blender. Note: the as-designed volume fraction (VF) differs slightly from the as-tested porosity (1 – VF) of the lattice due to resolution reductions in mesh quality through STL and CFD mesh generation.

Results Section	Test Descriptions	Reef Type	h [m]	R_c [−]	H [m]	T [s]	n [−]	S [−]	Avg. Reef Porosity [−]
3.1	Single-row SEAHIVE reefs	9-unit, 6-unit	0.6	−0.08	0.2	3.57	1	1	0.560–0.625
					0.3	4.47			
					0.4	5.37			
3.2	Single-row 6-unit lattice volume fraction reefs	VF55, VF50, VF45, VF40, VF35, VF30, VF25	0.6	−0.08	0.4	5.37	1	1	0.465–0.769
3.3	Three-row 6- and 9-unit combined SEAHIVE and lattice reefs	SEAHIVE-3row, Hybrid-3row-01, Hybrid-3row-02, …Hybrid-3row-26	0.6	−0.08	0.4	5.37	3	3	0.487–0.704
3.3	Top-performing three-row 6- and 9-unit combined SEAHIVE and lattice reefs	SEAHIVE-3row, Hybrid-3row-03, Hybrid-3row-04, Hybrid-3row-05, Hybrid-3row-14, Hybrid-3row-19, Hybrid-3row-24	0.6	−0.08	0.12	1.789	3	3	0.487–0.629
						2.683			
					0.25	2.683			
						4.472			
						5.367			
					0.4	5.367			

0.6 m (3.0 m) (Table 1). Subsequent cases used the most extreme wave condition (i.e., $H = 0.4$ m, $T = 5.37$ s) to assess reef performance and reduce the number of cases that needed to be run. The final hybrid reef cases used a wider range of wave conditions to assess the top performing three-row reef designs against characteristic waves at this deployment depth ($h = 3.0$ m).

2.5. Model data analysis and performance metrics

The performance of the hybrid reef designs was determined using three metrics, the wave transmission coefficient K_t [−], the wave reflection coefficient K_r [−] and the wave energy reduction $(1 - K_t^2)$. The wave transmission coefficient is defined as $K_t = \overline{H_t}/\overline{H_i}$, where $\overline{H_i}$ [m] is the temporal mean wave height in front of the reef structures, and $\overline{H_t}$ [m] is the temporal mean wave height at the rear of the structures. The reflection coefficient is defined as $K_r = \overline{H_r}/\overline{H_i}$, where $\overline{H_r}$ is the temporal mean reflected wave height in front of the reef structures. In general, the energy conservation equation is $K_t^2 + K_r^2 + K_d^2 = 1$ with K_d the component of energy dissipated inside the reef. The transmitted wave height is reduced when interacting with a submerged reef due to both reflection and internal dissipation (K_r^2+K_d^2), and hence the fraction of wave energy attenuated by the reef is $(1 - K_t^2)$. In other words, wave energy reduction refers to energy loss as waves propagate forwards across the reefs.

Here, in all cases, the extracted water level time series was split into incoming and outgoing signals (e.g., Guza et al., 1984) prior to estimating the modeled wave height at each sample position. To estimate K_t, each model was sampled for the free surface position and velocity profile one-half wavelength before the first reef to calculate $\overline{H_i}$ and $\overline{H_r}$, and one-half wavelength from the last reef to calculate $\overline{H_t}$.

The percentage wave energy reduction was estimated as

$$\text{Wave Energy Reduction } (\%) = \left(1 - K_t^2\right)*100. \quad (6)$$

3. Results

The following sections describe the results for the four tests conducted with the NWT (Table 1) to explore the hydrodynamic performance of the two sub-unit systems both in isolation and then together as a three-row hybrid reef system.

3.1. Single-row SEAHIVE reef

A single row of the 6- and 9-unit SEAHIVE reefs for a range of wave heights ($H = 0.2$ m–0.4 m) and periods ($T = 3.57$ s–5.37 s) show better performance (lower K_t and higher wave energy reduction) with larger waves and shorter wave periods for both the 6- and 9-unit reefs (Fig. 4). Due to the shallow freeboard, waves broke across the reef under the tested conditions. K_r does not depend on wave period, but weakly depends on the wave height, with greater reflectivity under smaller waves, indicating more flow over the reefs under larger waves. Comparing the 6- and 9-unit reefs, the larger 9-unit reefs produced lower K_t, higher K_r, and higher wave energy reduction values than the 6-unit reefs for the same set of wave conditions. This design has both a larger floor and crest width, and hence more material with which to interact, reflect, and reduce incident wave energy.

The specific dissipation rate (ω) [s^{-1}] was calculated by the $k - \omega$ *SST* turbulence model, where high values indicate areas with intense turbulence. These results show that the SEAHIVE reef allows water to flow into and out of the structure through perforations in the leading and trailing faces of the reef (Fig. 5). In this way, the SEAHIVE reef acts as a 'dissipation chamber' of wave energy. As a wave breaks across the reef, turbulence occurs inside the reef as water flows into it (Fig. 5b,c,g,h). Water is then ejected out of both the top and trailing face of the structure as the broken wave passes (Fig. 5d–i). As a result, there is a flow separation in the wake of the reef where a recirculation zone forms (Fig. 5e–j).

3.2. Single-row lattice reef

In this study, the SEAHIVE sub-units had a fixed porosity while the porosity of the lattices ranged from 0.769 to 0.465 for VF 25–55% (Table 1). These 6-unit reefs were tested with waves $H = 0.4$ m high and periods of $T = 5.37$ s (Fig. 6). K_t varies inversely (Fig. 6a), and K_r directly (Fig. 6b) with VF for the lattice cases. These effects are explained by a decrease in the porosity of the lattice with increasing VF, resulting in lower wave transmission and greater reflectivity. Similarly, the wave energy reduction (Fig. 6c) also increased with VF, but rolled off around VF50, where the difference in energy reduction between VF50 and VF55

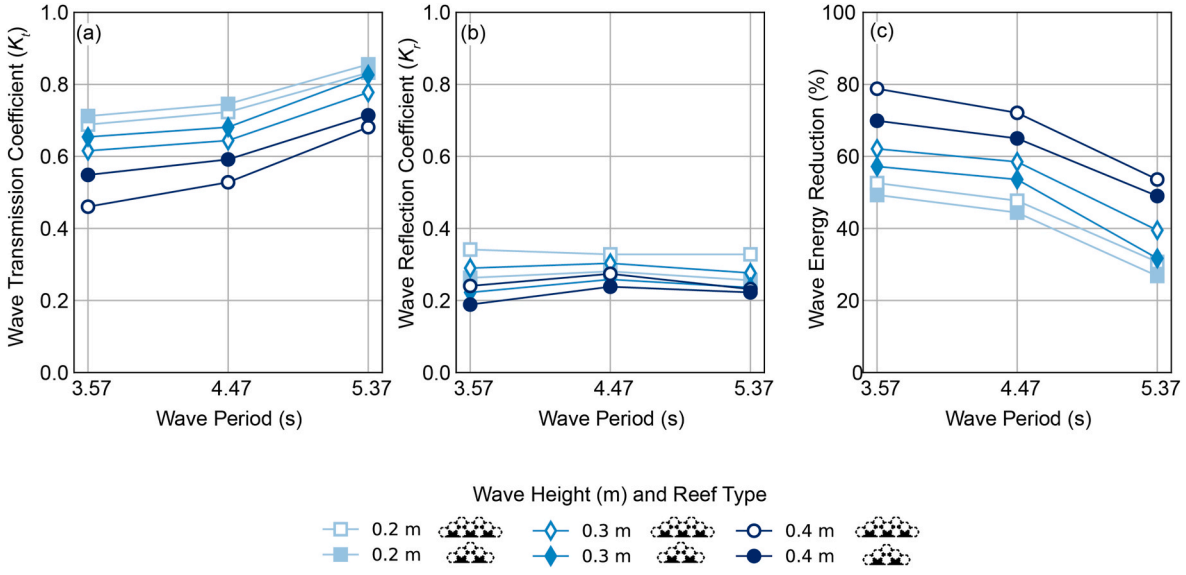

Fig. 4. Mean values of the wave height transmission factor, K_t (a), reflection factor, K_r (b), and percent wave energy reduction (c) for 6- and 9-unit single-row SEAHIVE reefs under different wave heights (colors) and periods. In this figure, filled symbols correspond to the 6-unit SEAHIVE design, and open symbols the 9-unit SEAHIVE design. Note, better performance corresponds to lower values of K_t and higher values of wave energy reduction. (For interpretation of the references to color in this figure legend, the reader is referred to the Web version of this article.)

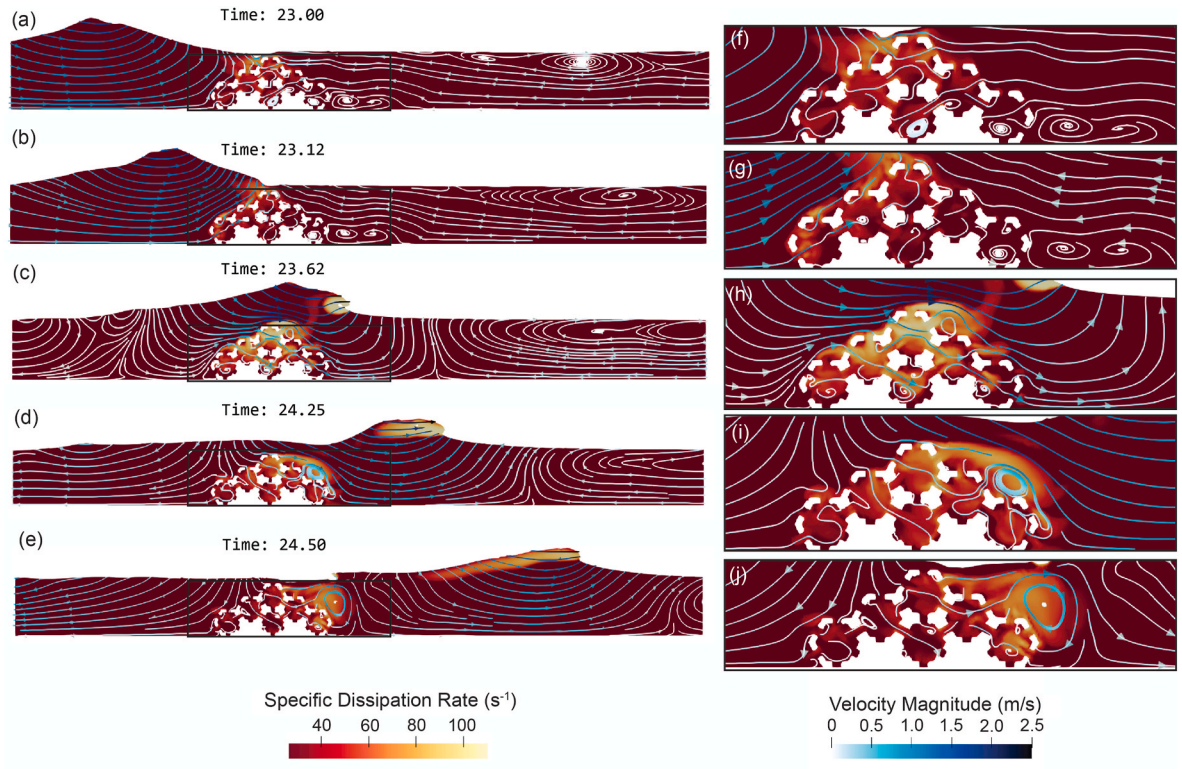

Fig. 5. Five timesteps (a–e) of a cross-section from one of the 6-unit SEAHIVE NWT models showing a single wave crest passing over the reef structure. In this figure, the incident wave condition is $H = 0.4$ m, $T = 5.37$ s. Insets (f–j) show a close-up of the flow inside the SEAHIVE reef. Here, the velocity magnitude is represented by streamlines (blue colors) where the directionality of flow is shown by small arrows on each streamline. Streamlines are tangential to the instantaneous velocity direction and denote the direction a particle of water would move at a given instance in time. The specific dissipation rate (red colors) indicates where turbulence occurs as the wave interacts with the reef structure. (For interpretation of the references to color in this figure legend, the reader is referred to the Web version of this article.)

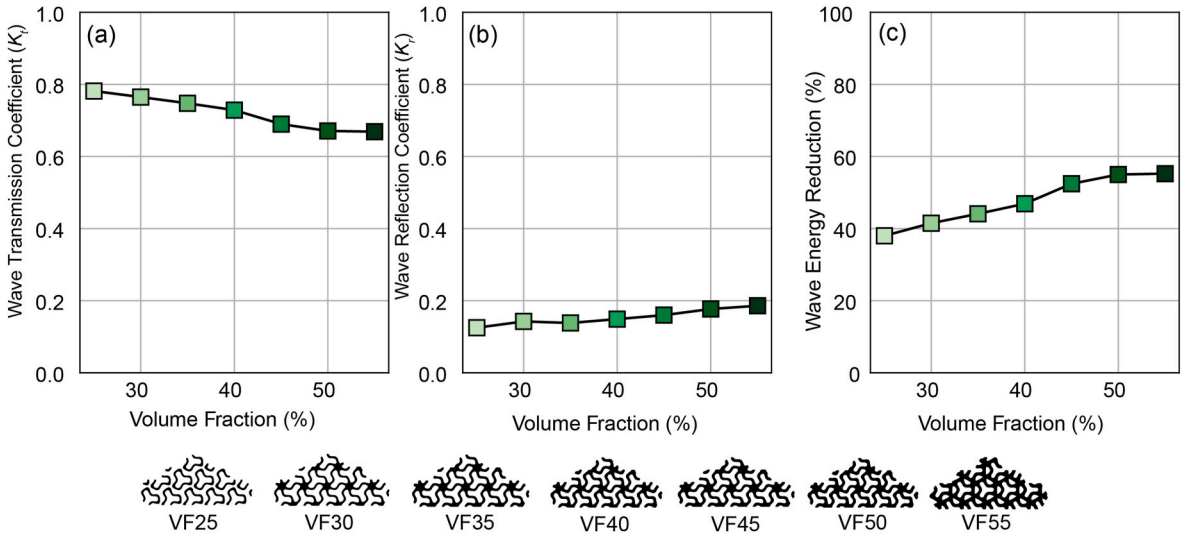

Fig. 6. Mean values of the wave height transmission factor, K_t (a), reflection factor, K_r (b), and percent wave energy reduction (c) for lattice reefs with volume fractions (VF) 25%–55% at steps of 5% under constant wave conditions ($H = 0.4$ m, $T = 5.37$ s). Note, higher performance corresponds to lower values of K_t and higher values of wave energy reduction. As the reef performance rolls off with increasing VF, 55% was determined to be the optimal setting for the lattice reef design.

is negligible (~1%). Therefore, the results indicate that a VF beyond 55% should result in minimal performance gains. The VF55 lattice has the lowest K_t and highest K_r of the designs considered, and these values are near that of the 6-unit SEAHIVE reef for the same wave conditions (i.e., compare Fig. 4a and b and Fig. 6a and b). These slight performance gains are likely related to porosity; the VF55 lattice has a porosity of 0.465 while the same SEAHIVE is 0.625. Hence, the lattice may be a tunable feature that can be used to channel water through the reef depending on its placement within the larger reef structure.

Under the same wave forcing, the 6-unit VF55 lattice reef dissipates a similar amount of wave energy as the 6-unit SEAHIVE reef (e.g., Figs. 4c and 6c), but has different internal flow characteristics. Under a wave

crest, water enters the lattice via holes in its leading edge and is channeled through the reef in helical, non-intersecting channels, creating a layered-flow effect (Fig. 7). The directionality of flow within the lattice depends on the position of the wave crest and hence the pressure field; some water is forced out of the top of the trailing edge of the lattice reef while other water is forced towards its base.

This channelization first creates high turbulence in the leading edge of the lattice (Fig. 8e) as water both enters the reef structure and is forced over the top of the reef, steepening the wave crest and causing the wave to break. As water is ejected from the lee side of the lattice, a recirculation zone forms as the wave passes overhead (Fig. 8f). These properties are advantageous in reef design as the lattice can be used as a primary dissipator of energy (either with placement on the leading or trailing edges, or at the crest of a reef). Since SEAHIVE sets up stronger internal dissipation (Fig. 5), this sub-unit best functions as the core of the reef, both dissipating energy and providing flow conductivity between the exterior lattice elements.

3.3. Hybrid SEAHIVE-lattice reefs

Given their different flow properties, the combination of the two sub-unit systems into a hybrid reef structure may provide better performance by both enhancing internal dissipation while redirecting flow in the top of the reef structure (Fig. 9). Flow in the lattice 'armor' on the sides of a 3-unit SEAHIVE reef (Fig. 9d–f) generates high leading-edge turbulence as well as a disruption of the passing wave crest, resulting in steepening as the wave passes overhead, relative to the SEAHIVE-only design (Fig. 9a–c). Accordingly, the hybrid design has better performance than the SEAHIVE-only design: K_t = 0.59 versus 0.67; and wave energy reduction = 65% versus 55%.

The hybrid reefs were constructed by arranging SEAHIVE and lattice sub-units in different 6- and 9-unit configurations, replacing SEAHIVE sub-units with lattice on the top and sides of the reef units (Supplementary Materials). Starting with a 6-unit SEAHIVE-3row design, 24 hybrid configurations were created by replacing either the first and second, second and third, or first and third reefs with hybrids (Fig. 10). In addition to these 6-unit, three-row reefs, two tests were run by replacing the first and then all rows with 9-unit hybrids. These 27 cases (including the SEAHIVE-3row design) were run in the NWT using the maximum (conservative) wave height of H = 0.4 m and T = 5.37 s, and then the top 7 designs were selected (Fig. 11) to run through a wider range of wave conditions, H = 0.12–0.4 m (0.6–2.0 m prototype scale) and T = 1.79 s–5.37 s (4.0–12.0 s) while maintaining a constant freeboard of −0.08 m (−0.4 m) to improve the granularity of the results (Fig. 12).

Such comparison demonstrates that the best overall design across all wave conditions was 'hybrid-3-row-2' (Fig. 12), as it has the most material for water to interact with and hence reduce incident wave energy. However, the other designs also had high performance for certain wave conditions, suggesting that the geometry of the reef units also contributes to their performance. Indeed, from a cost perspective, hybrid-3row-1′ may provide a better solution, due to its generally high performance and lower number of sub-units than 'hybrid-3row-2' (i.e., 27 versus 21 sub-units, respectfully). In general, most three-row designs had higher performance when the third-row position was occupied by a SEAHIVE reef and indeed, the 'SEAHIVE-3row' design had high performance across all tested conditions. This result is due to the porous SEAHIVE design allowing water to easily permeate into the structure, thereby

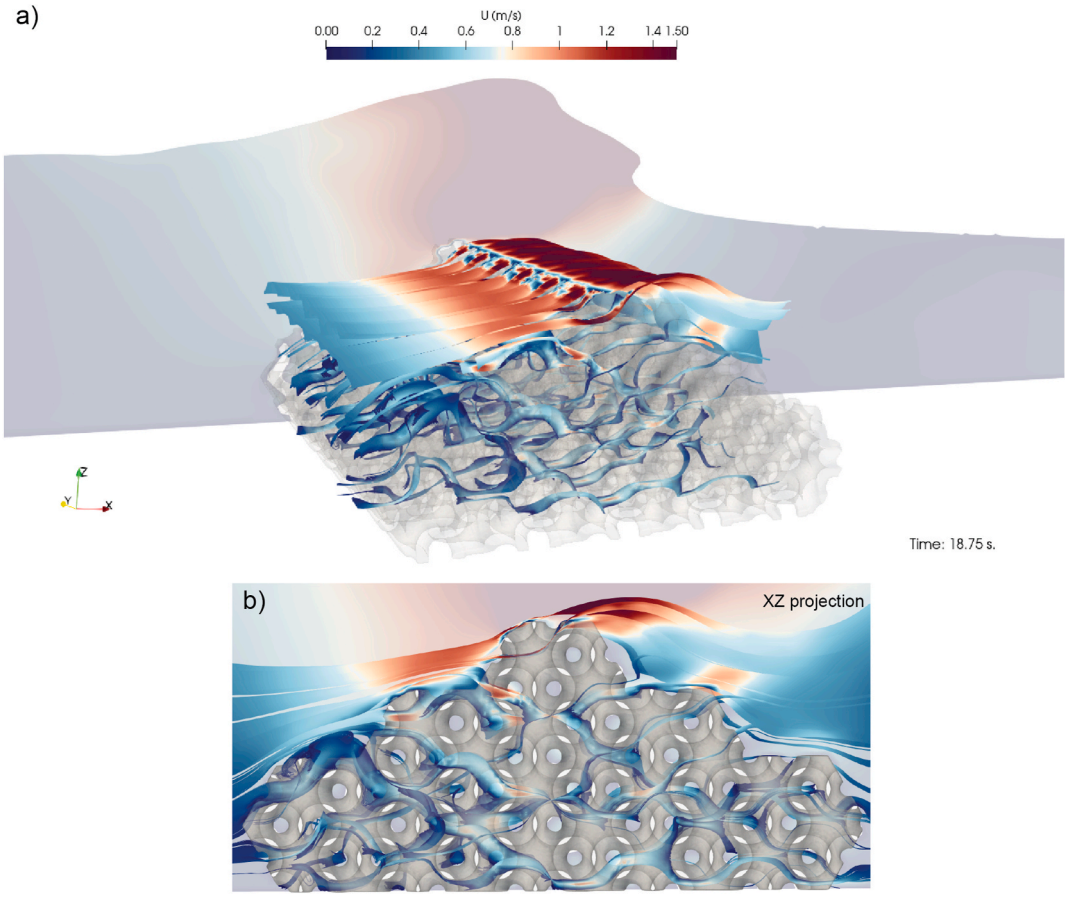

Fig. 7. Visualization of flow through the lattice structure under a wave crest. Here, streamlines are colored by the velocity magnitude which demonstrate a layered-flow effect through the lattice structure. The 'offshore' direction is to the left side of the figure and the 'onshore' direction is to the right. Water enters the reef through holes on the leading edge of the lattice and then gets redirected through the structure via helical pathways that do not intersect.

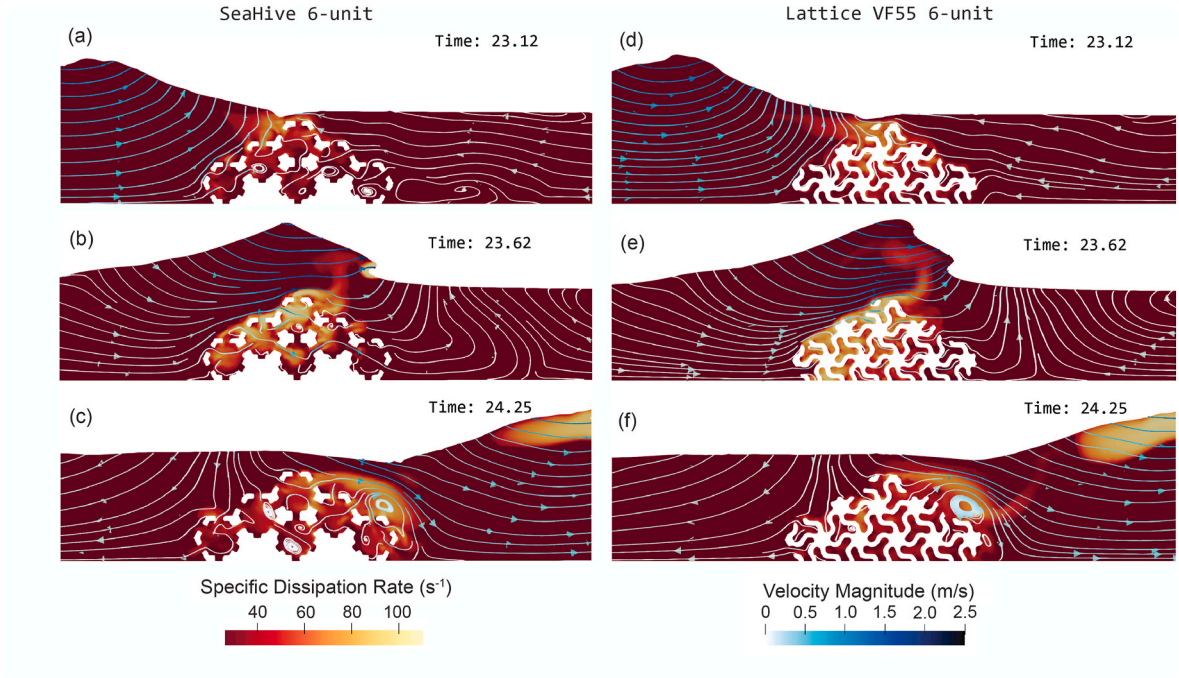

Fig. 8. Three timesteps from the NWTs showing a wave passing over the 6-unit SEAHIVE (a–c) and 6-unit VF55 lattice (d–f) reefs. In this figure, the incident wave condition is $H = 0.4$ m, $T = 5.37$ s. Here, the velocity magnitude is represented by streamlines (blue colors) where the directionality of flow is shown by small arrows on each streamline. The specific dissipation rate (red colors) indicates where turbulence occurs as the wave interacts with the reef structure. In comparison with the SEAHIVE reef, the lattice reef steepens the wave crest and generates a stronger eddy in the lee of the structure as the wave passes. For the SEAHIVE reef, $K_t = 0.72$, $K_r = 0.22$, and wave energy reduction = 48%. For the lattice reef, $K_t = 0.67$, $K_r = 0.19$, and wave energy reduction = 55%. (For interpretation of the references to color in this figure legend, the reader is referred to the Web version of this article.)

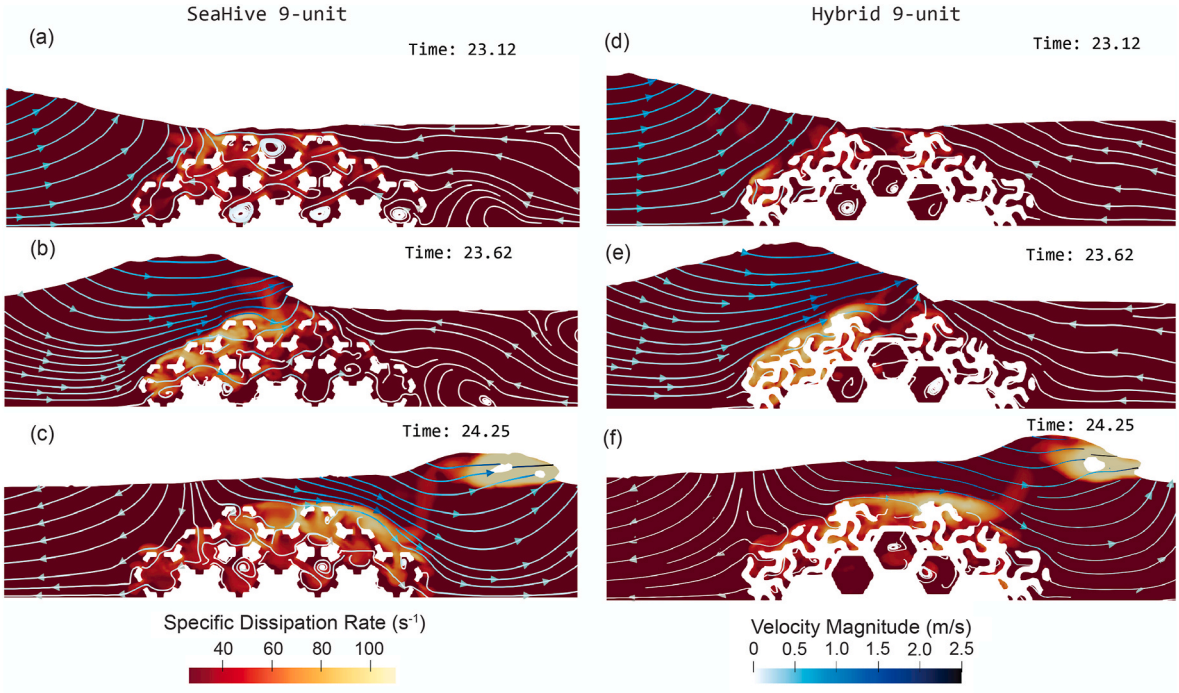

Fig. 9. Three timesteps from the CFD model comparing the 9-unit SEAHIVE (a–c) and hybrid SEAHIVE-lattice (d–f) reefs. In this figure, the incident wave condition is $H = 0.4$ m, $T = 5.37$ s. Here, the velocity magnitude is represented by streamlines (blue colors) where the directionality of flow is shown by small arrows on each streamline. The specific dissipation rate (red colors) indicates where turbulence occurs as the wave interacts with the reef structure. The hybrid reef combines the performance attributes of both the SEAHIVE and lattice systems. For the SEAHIVE reef, $K_t = 0.67$, $K_r = 0.24$, and wave energy reduction = 55%. For the hybrid reef, $K_t = 0.59$, $K_r = 0.21$, and wave energy reduction = 65%. (For interpretation of the references to color in this figure legend, the reader is referred to the Web version of this article.)

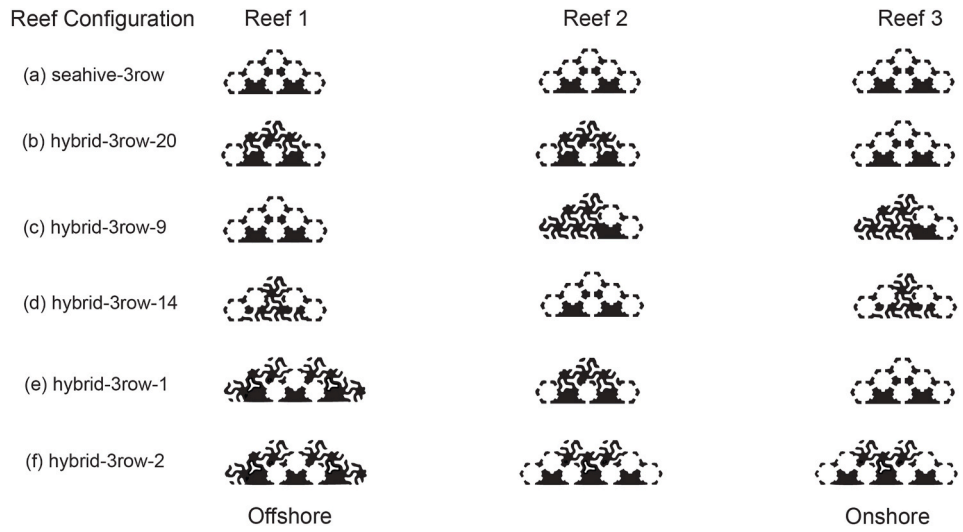

Fig. 10. Example reef configurations for the hybrid 3-row cases, with a SEAHIVE-only design (a), and hybrid designs replacing the first and second reefs (b), second and third reefs (c), and first and third reefs (d). Also shown are two designs featuring the larger 9-unit hybrid reef, first as just the offshore reef (e) and then as all three reefs in the configuration (f).

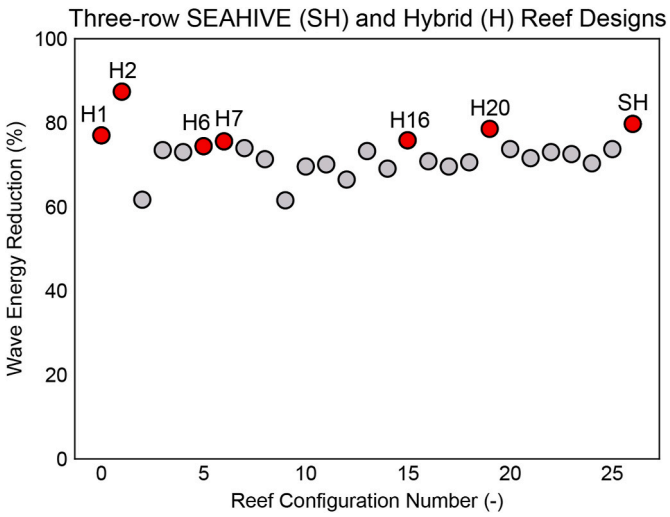

Fig. 11. Wave energy reduction values under the maximum wave condition (H = 0.4 m, T = 5.37 s) for the three-row SEAHIVE-3row (SH) and hybrid-3row (H) configurations, where the number corresponds to the unique configuration (Fig. 10). The top seven designs with the highest energy reduction values (red markers) were chosen for further performance testing under a wider range of wave conditions (Fig. 12). (For interpretation of the references to color in this figure legend, the reader is referred to the Web version of this article.)

dissipating the remainder of the wave bore as it passes over the structure (e.g., Figs. 8 and 9). However, the inclusion of the lattices in the hybrid reef reduces the wave reflection relative to the SEAHIVE design (e.g., comparing Figs. 4 and 6; Fig. 9). Hence, this benefit of the hybrid design may be useful in coastal applications that seek to reduce reflected wave energy and instead increase internal energy dissipation within the reef structure itself.

While many hybrid designs had high wave energy reduction values between 70 and 90%, several designs, including the 'hybrid-3row-1' and 'hybrid-3row-2' designs, also produced lower wave energy reduction values (50–60%) under certain wave conditions. This pattern may be due to the specific configuration of the two sub-unit systems in these cases as this pattern was not consistent across all designs and tested conditions (e.g., for the H = 0.25 m, T = 5.37 s condition, hybrid-3row-20 produced an energy reduction value of 68.0% whereas hybrid-3row-16 produced 53.1%). Regardless, it can be concluded that these hybrid reefs can produce high levels of wave energy reduction, commensurate with existing designs for submerged reef breakwaters as well as natural coral reefs (e.g., Goda and Ahrens, 2009; Lowe et al., 2005). The reef sub-units can be rearranged into different combinations to tune the energy reduction values and hence match the needs of different coastal environments.

Examining the hybrid reef performance across the parameter space R_c/H_i and K_t suggests these designs are comparable to empirical wave flume data from Van Gent et al. (2023) for impermeable, rubble mound, and perforated LCS under the same wave period of T = 5.37 s (Fig. 13). To make the results of the present study consistent with the empirical formulas from Van Gent et al. (2023), we recalculated H at four positions in the models, before the first reef (H_1), between the first and second reefs (H_2), between the second and third reefs (H_3), and after the third reef, to calculate an effective K_t for each row (denoted in Fig. 13 as $K_{t\,(1,2,3)}$). Across all hybrid designs, most wave attenuation occurs at the first reef (K_t = 0.50 to 0.72), with similar attenuation for the second and third reefs (K_t = 0.65 to 0.88). These values are between the expected range of performance for the perforated and rubble mound breakwater designs from Van Gent et al. (2023). Two of the 'final' 9-unit hybrid reef designs (colored symbols in Fig. 13) have similar performance values with the singular impermeable breakwater design from Van Gent et al. (2023) for this range of R_c/H_i, and are also noticeably different in performance from the other hybrid reef designs. These results imply that the empirical expression (Eq. (6)) in Van Gent et al. (2023) may also be applicable for the multi-row artificial reef designs developed here, after accounting for the change in wave height across each of the reefs.

4. Discussion

This study developed and tested a novel artificial reef system using CFD as a hydrodynamic performance assessment tool. Relative to wave tanks, conducting performance analysis in CFD has some advantages, namely that the CFD tool allowed for a relatively efficient assessment of different design considerations once the initial model domain had been developed. This method allowed us to consider a wide range of different possible design choices with the SEAHIVE and lattice systems without the need for physically constructing all the sub-units. Yet, the CFD simulations were limited by computational complexity, and the models had to be simplified with flat bathymetry, narrow along-shore sections, and use monochromatic waves to reduce model runtimes. Future work

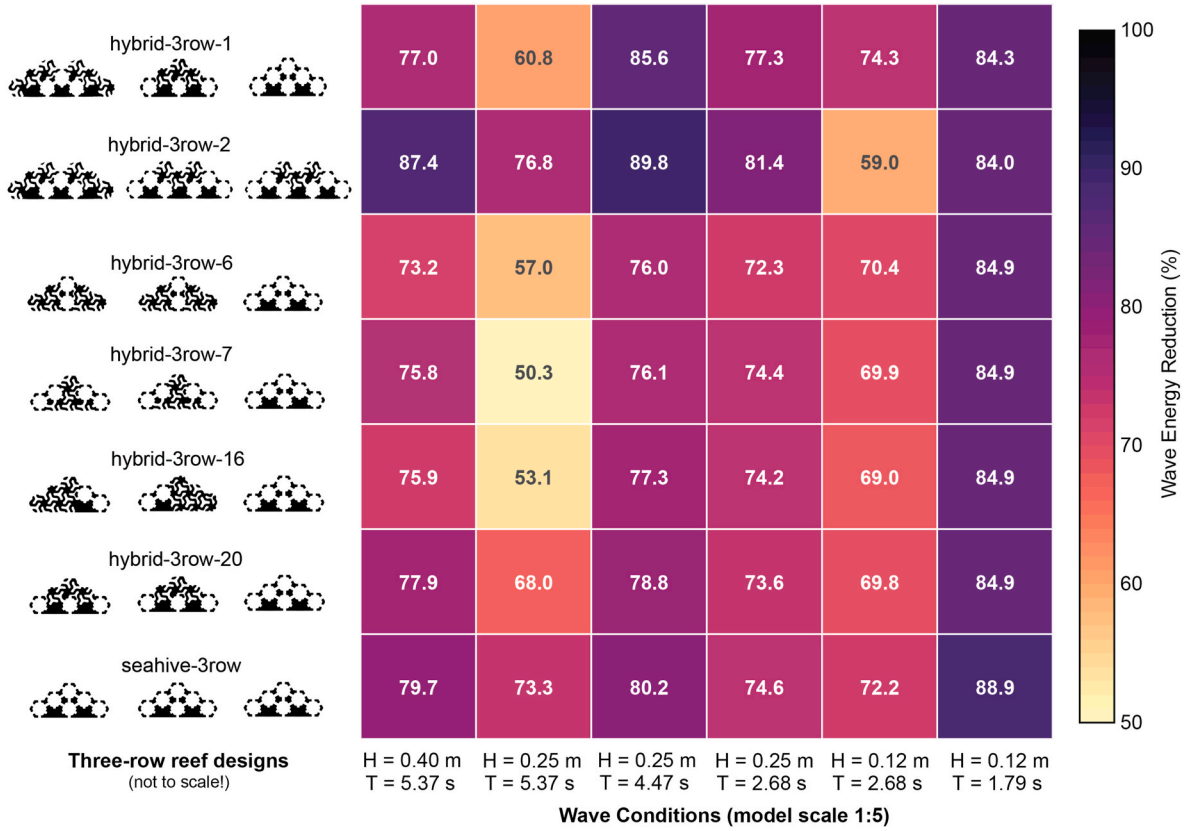

Fig. 12. Performance matrix for six hybrid reef and one SEAHIVE three-row layouts under a range of wave conditions (Table 1). Here colors correspond to the percent wave energy reduction, with exact values printed in each cell of the matrix. In general, including either the larger 9-unit hybrid reefs, or a SEAHIVE reef in the third-row position, resulted in better performance (higher wave energy reduction) across the range of tested wave conditions. (For interpretation of the references to color in this figure legend, the reader is referred to the Web version of this article.)

will test the designs presented in Fig. 12 in a wave flume to calibrate the CFD model, enable further design iteration, and provide further insight into the flow-field effects of these hybrid reefs.

Here, each design was assessed using standard approaches for low-crested structures (LCS), i.e., K_t and K_r, respectively, as well as the wave energy reduction ($1 - K_t^2$) of the reefs. The simulations also demonstrate that the SEAHIVE and lattice sub-units can modify the flow properties of a traditional reef breakwater, allowing water to flow over and through the structure through specific, engineered pathways. The K_t of each design was generally a good predictor of its wave energy reduction, and designs with greater wave energy reduction had proportionally lower K_t and larger K_r (Figs. 4 and 6), indicating these simple metrics could be relevant for describing hybrid reef performance. However, these K_r values are lower than expected for traditional impermeable or rubble-mound breakwaters (e.g., Ahrens and Cox, 1990; Van Gent et al., 2023), suggesting that K_r may be a limited predictor of the total wave energy reduction across these type of multi-row, highly porous reefs (e.g., van den Brekel, 2021). Comparisons of the empirical formulas presented in Van Gent et al. (2023) indicate that the hybrid reef designs explored here are within the expected range of K_t for the parameter space R_c/H_i, commonly used to describe the performance of LCS. As the present study considered a limited set of reef arrangements, future work may consider optimizing porous artificial reefs to enhance reflection, if this is a desired outcome, through selective placement of reflective sub-units.

While the focus of this work was to develop multi-row hybrid reef designs for wave energy reduction, such designs are also intended to provide co-benefits like refugia for benthic organisms, enabling the cultivation of corals. From the CFD model results, velocities within the reef units varied between ~0.1 and 0.5 m/s at 1:5 scale (0.22–1.1 m/s at prototype scale), with higher internal velocities associated with the SEAHIVE reefs (Figs. 5, 8 and 9). Indeed, combining the SEAHIVE and lattice sub-units together resulted in lower internal velocity and turbulence (e.g., Fig. 9d–f) that may be suitable for coral colonization. Turbulence within coral reef environments plays a vital role in facilitating larval dispersal and mixing nutrients, but may also cause the dislodgement of settled larva if shear stresses across the reef are too intense (Reidenbach et al., 2021; Stocking et al., 2016). Thus, porous artificial reefs that generate both high levels of turbulence due to wave energy dissipation as well as lower internal turbulence due to their physical structure, may provide ample coastal protection and this desired outcome for benthic organisms. Furthermore, a multi-reef design has advantages over a single reef in that the offshore reef may provide much of the wave energy reduction (e.g., Fig. 13), while the inshore reefs may provide suitable areas for coral cultivation. These key aspects of hybrid reef design should be explored in future research.

In general, it is expected that an impermeable reef design will reduce wave transmission relative to a permeable design due to the high amount of wave reflection that occurs off such a structure. Yet, if a permeable design is optimized for internal energy dissipation, then it can have similar performance as an impermeable structure (this is shown experimentally in Van Gent et al., 2023). Here, several porous reef designs are developed that achieve a similar level of performance as an impermeable reef (Fig. 13) by optimizing both reflection as well as internal dissipation. Traditional, (relatively) impermeable rubble-mound breakwaters can cause unintended consequences, such as the pooling of water in the nearshore, sometimes leading to poor water quality and unnatural beach morphology (e.g., Penchev, 2005). Highly porous reef designs have the potential to remedy such issues by allowing water to flow more freely through the structure, setting up a more

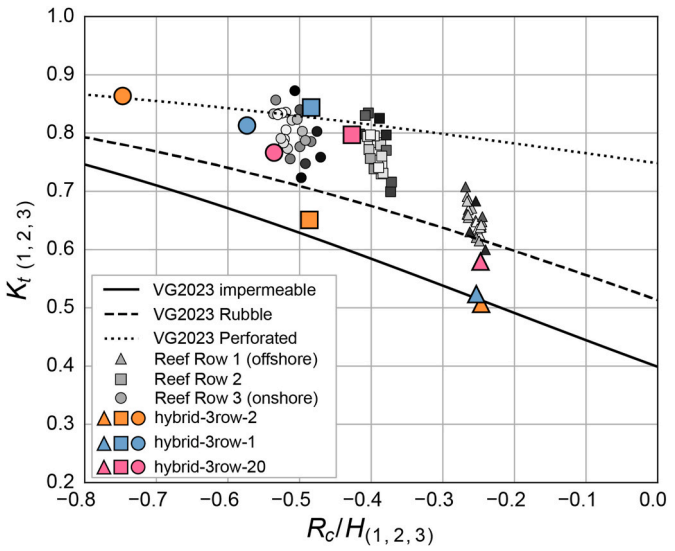

Fig. 13. Comparison of experimental data by Van Gent et al. (2023) for their impermeable, rubble mound, and perforated trapezoidal reef designs (black lines) and the three-row hybrid reef designs (Figs. 11 and 12), where grey to black triangles are the K_t values of the first row, squares the second row, and circles the third row. Also shown are the three top-performing designs as colored symbols: hybrid-3row-2 (orange symbols), hybrid-3row-1 (blue symbols), and hybrid-3row-20 (pink symbols). For consistency with the single-row reef designs in Van Gent et al. (2023), we recalculated the wave transmission coefficient K_t between the first and second reef (Row 1), second and third reefs (Row 2), and after the third reef (Row 3). With these multi-row reef designs, most of the wave height reduction occurs after the first reef, with the second and third reefs contributing less wave height reduction. (For interpretation of the references to color in this figure legend, the reader is referred to the Web version of this article.)

natural coastal circulation pattern, while still providing coastal defense from larger waves. Future work should include assessing the coastal hazard risk reduction (i.e., nearshore hydrodynamics and wave runup) of these types of structures, based on the structure's location relative to shore, nearshore bathymetry, and local wave climate. Such analyses will require specific knowledge of the environmental conditions at the intended deployment site.

Finally, it should be noted that a meaningful cost comparison of these reef designs cannot be conducted without detailed information on factors such as design complexity, project scale, site location, manufacturing and deployment methods, and material selection which drive the installed cost of the LCS. However, the reef designs investigated in this paper exhibit porosities ranging from 0.47 to 0.77, potentially leading to substantial material cost savings compared to traditional rubble-mound breakwaters, particularly for larger-scale projects. Furthermore, the ability to specifically route water through the hybrid reefs may prove beneficial for large-scale reef restoration. Both the SEAHIVE and lattice sub-units can be cast or 3D printed in concrete. Cost reduction can be achieved by 3D printing, either entire reef sections, or three-sub-unit sections. Such sub-unit clustering could lower deployment costs as there would be fewer reef units to install in the ocean.

5. Conclusions

This study compares a series of novel artificial reef systems according to their hydrodynamic performance in a numerical wave tank (NWT) using computational fluid dynamics (CFD) under different idealized, representative, wave conditions. The artificial reefs were composed of two interlocking systems based on a hexagonal sub-unit, SEAHIVE and lattice. The purpose of this work was to determine how different prototype artificial reef designs could be tested to understand their performance in terms of the forward propagating wave energy reduction across the reef units, compared with other LCS, and the effects of various combinations of sub-units on flow patterns within and above the reefs. After initial testing with two-dimensional (2D) CFD models to determine the ideal reef freeboard, number of rows, and row spacing, a series of three-dimensional (3D) models were developed to test the reefs as single and then in three-row configurations.

Reefs made of 6 SEAHIVE sub-units tended to reduce wave energy less than reefs made of 9 SEAHIVE sub-units. The reefs also differ in terms of their fluid dynamics. A visualization of CFD results shows that water penetrates inside the SEAHIVE reef through perforations in its outer edge, setting up internal circulation within the reef structure that dissipates energy as turbulence. The lattice is composed of many helical channels that redirect water through its structure, generating lower internal turbulence but higher exit velocities than the SEAHIVE sub-units. When the volume fraction (VF) of the lattice sub-units is large (55%), they reduce more wave energy than the corresponding SEAHIVE sub-units. Hence, successful hybrids of the two sub-unit systems typically featured lattices placed either at the front or at the top of the reef, allowing the lattice to break up the incoming wave and the SEAHIVE to dissipate it by setting up internal eddies. Importantly, these hybrids generate lower internal turbulence than a SEAHIVE-only design, an aspect that may be important for ecological engineering with such artificial reefs.

Of the 27 three-row hybrid reef designs that were tested, three resulted in wave energy reduction values between 70 and 90%, commensurate with existing submerged breakwater designs and natural coral reefs. Future work will be conducted to improve upon these designs and will consider aspects such as: shear stress and drag created by reef units, their stability, and suitability for coral cultivation, cost optimization, and deployment considerations.

CRediT authorship contribution statement

Benjamin K. Norris: Writing – review & editing, Writing – original draft, Visualization, Software, Project administration, Methodology, Investigation, Formal analysis, Data curation, Conceptualization. **Borja G. Reguero:** Writing – review & editing, Validation, Supervision, Project administration, Methodology, Investigation, Funding acquisition. **Joseph Bartolai:** Writing – review & editing, Writing – original draft, Methodology, Investigation, Formal analysis, Data curation. **Michael A. Yukish:** Supervision, Project administration, Methodology, Funding acquisition, Conceptualization. **Landolf Rhode-Barbarigos:** Writing – review & editing, Writing – original draft, Supervision, Methodology, Funding acquisition, Data curation, Conceptualization. **Brian K. Haus:** Writing – review & editing, Supervision, Project administration, Funding acquisition, Conceptualization. **Gabriel Barajas Ojeda:** Writing – review & editing, Visualization, Validation, Supervision, Software, Methodology. **Maria Maza:** Writing – review & editing, Supervision, Resources, Conceptualization. **Javier L. Lara:** Supervision, Conceptualization. **Michael W. Beck:** Supervision, Project administration, Funding acquisition.

Declaration of competing interest

The authors declare the following financial interests/personal relationships which may be considered as potential competing interests: Declarations of interest: none.

Acknowledgements

The authors would like to acknowledge the contribution of the larger X-REEFS team in developing the reef concepts explored in this study, and in particular Andrew Baker, Prannoy Suraneni, and Sanchit Mehta (University of Miami); Taylor Squires, Laura Cherney, David Moulton,

Ramon Mendieta and Craig Raffenberg (AECOM). Funding for this project was provided by the United States Defense Advanced Research Projects Agency (DARPA) under Grant no. HR001121S0012-FP-021: REEFS (Reef Engineering to Enhance Future Structures). The authors (BKN, BGR, MWB) would like to acknowledge additional support from the United States Army Corps of Engineers (USACE) Engineering With Nature (EWN) program under Grant no. W912HZ-24-2-0004.

Appendix A. Supplementary data

Supplementary data to this article can be found online at https://doi.org/10.1016/j.coastaleng.2025.104742.

Data availability

Data will be made available on request.

References

Ahrens, J.P., 1984. Reef type breakwaters. Coastal Engineering Proceedings 178–179. https://doi.org/10.9753/icce.v19.178.

Ahrens, J.P., Cox, J., 1990. Design and performance of reef breakwaters. J. Coast Res. 61–75.

Asif, M., Muneer, T., 2007. Energy supply, its demand and security issues for developed and emerging economies. Renew. Sustain. Energy Rev. 11, 1388–1413. https://doi.org/10.1016/j.rser.2005.12.004.

Barber, T., Krumholz, J., 2007. A step-by-step guide for grassroots efforts to reef rehabilitation. The Reef Ball Foundation. Inc, Athens, GA.

Barnard, P.L., Erikson, L.H., Foxgrover, A.C., Hart, J.A.F., Limber, P., O'Neill, A.C., van Ormondt, M., Vitousek, S., Wood, N., Hayden, M.K., Jones, J.M., 2019. Dynamic flood modeling essential to assess the coastal impacts of climate change. Sci. Rep. 9, 1–13. https://doi.org/10.1038/s41598-019-40742-z.

Beck, M.W., Lange, G.M. (Eds.), 2016. Managing Coasts with Natural Solutions: Guidelines for Measuring and Valuing the Coastal Protection Services of Mangroves and Coral Reefs. World Bank Group, Washington D.C.

Cooper, J.A.G., Pilker, O.H., 2012. Pitfalls of Shoreline Stabilization. Springer Science & Business Media.

Dafforn, K.A., Glasby, T.M., Airoldi, L., Rivero, N.K., Mayer-Pinto, M., Johnston, E.L., 2015. Marine urbanization: an ecological framework for designing multifunctional artificial structures. Front. Ecol. Environ. 13, 82–90. https://doi.org/10.1890/140050.

Di Paolo, B., Lara, J.L., Barajas, G., Losada, Í.J., 2021. Wave and structure interaction using multi-domain couplings for Navier-Stokes solvers in OpenFOAM®. Part I: Implementation and validation. Coast. Eng. 164, 103799. https://doi.org/10.1016/j.coastaleng.2020.103799.

Diederen, C., 2022. Experimental Wave Flume Study: the Stability of an Artificial Reef (Masters Thesis). TU Delft, Faculty Civil Engineering & Geosciences. Civil Engineering & Geosciences.

Ferrario, F., Beck, M.W., Storlazzi, C.D., Micheli, F., Shepard, C.C., Airoldi, L., 2014. The effectiveness of coral reefs for coastal hazard risk reduction and adaptation. Nat. Commun. 5, 1–9. https://doi.org/10.1038/ncomms4794.

Fisher, J.W., Miller, S.W., Bartolai, J., Simpson, T.W., Yukish, M.A., 2023. Catalog of triply periodic minimal surfaces, equation-based lattice structures, and their homogenized property data. Data Brief 49, 109311. https://doi.org/10.1016/j.dib.2023.109311.

Ghiasian, M., Rossini, M., Amendolara, J., Haus, B., Nolan, S., Nanni, A., Bel Had Ali, N., Rhode-Barbarigos, L., 2019a. Test-driven design of an efficient and sustainable Seawall structure. https://doi.org/10.18451/978-3-939230-64-9_122.

Ghiasian, M., Rossini, M., Nanni, A., Haus, B., Nolan, S., Rhode-Barbarigos, L., 2019b. Towards the Experimentally Based Design of an Effective and Ecofriendly Modular Shoreline Protection System for High Energy Tidal Flow.

Goda, Y., Ahrens, J.P., 2009. New formulation of wave transmission over and through low-crested structures. In: Coastal Engineering 2008. World Scientific Publishing Company, pp. 3530–3541. https://doi.org/10.1142/9789814277426_0293.

Guza, R.T., Thornton, E.B., Holman, R.A., 1984. Swash on Steep and shallow Beaches. Coastal Engineering Proceedings 48–49. https://doi.org/10.9753/icce.v19.48.

Higuera, P., Lara, J.L., Losada, I.J., 2014. Three-dimensional interaction of waves and porous coastal structures using OpenFOAM®. Part I: formulation and validation. Coast. Eng. 83, 243–258. https://doi.org/10.1016/j.coastaleng.2013.08.010.

Higuera, P., Lara, J.L., Losada, I.J., 2013. Realistic wave generation and active wave absorption for Navier-Stokes models. Application to OpenFOAM®. Coast. Eng. 71, 102–118. https://doi.org/10.1016/j.coastaleng.2012.07.002.

Hirt, C.W., Nichols, B.D., 1981. Volume of fluid (VOF) method for the dynamics of free boundaries. J. Comput. Phys. 39, 201–225. https://doi.org/10.1016/0021-9991(81)90145-5.

Jacobsen, N.G., Fuhrman, D.R., Fredsøe, J., 2012. A wave generation toolbox for the open-source CFD library: OpenFoam®. Int. J. Numer. Methods Fluid. 70, 1073–1088.

Jones, W.P., Launder, B.E., 1973. The calculation of low-Reynolds-number phenomena with a two-equation model of turbulence. Int. J. Heat Mass Tran. 16, 1119–1130. https://doi.org/10.1016/0017-9310(73)90125-7.

Larsen, B.E., Fuhrman, D.R., 2018. On the over-production of turbulence beneath surface waves in Reynolds-averaged Navier–Stokes models. J. Fluid Mech. 853, 419–460. https://doi.org/10.1017/jfm.2018.577.

Lowe, R.J., Falter, J.L., Bandet, M.D., Pawlak, G., Atkinson, M.J., Monismith, S.G., Koseff, J.R., 2005. Spectral wave dissipation over a barrier reef. J. Geophys. Res. C Oceans 110, 1–16. https://doi.org/10.1029/2004JC002711.

Maza, M., Lara, J.L., Losada, I.J., 2015. Tsunami wave interaction with mangrove forests: a 3-D numerical approach. Coast. Eng. 98, 33–54. https://doi.org/10.1016/j.coastaleng.2015.01.002.

Mendoza, E., Ríos, A., Mariño-Tapia, I., Silva, R., 2019. Modular coral shaped artificial reefs acting as beach protection barriers. https://doi.org/10.18451/978-3-939230-64-9_099.

Menter, F.R., 1994. Two-equation eddy-viscosity turbulence models for engineering applications. AIAA J. 32, 1598–1605. https://doi.org/10.2514/3.12149.

Monismith, S.G., Rogers, J.S., Koweek, D., Dunbar, R.B., 2015. Frictional wave dissipation on a remarkably rough reef. Geophys. Res. Lett. 42, 4063–4071. https://doi.org/10.1002/2015GL063804.

Moschella, P.S., Abbiati, M., Åberg, P., Airoldi, L., Anderson, J.M., Bacchiocchi, F., Bulleri, F., Dinesen, G.E., Frost, M., Gacia, E., Granhag, L., Jonsson, P.R., Satta, M.P., Sundelöf, A., Thompson, R.C., Hawkins, S.J., 2005. Low-crested coastal defence structures as artificial habitats for marine life: using ecological criteria in design. Coastal Engineering, Low Crested Structures and the Environment 52, 1053–1071. https://doi.org/10.1016/j.coastaleng.2005.09.014.

Penchev, V., 2005. Interaction of waves and reef breakwaters. In: Zimmermann, C., Dean, R.G., Penchev, V., Verhagen, H.J. (Eds.), Environmentally Friendly Coastal Protection. Springer, Netherlands, Dordrecht, pp. 107–127. https://doi.org/10.1007/1-4020-3301-X_7.

Pequignet, A.C., Becker, J.M., Merrifield, M.A., Boc, S.J., 2011. The dissipation of wind wave energy across a fringing reef at Ipan, Guam. Coral Reefs 30, 71–82. https://doi.org/10.1007/s00338-011-0719-5.

Pioch, S., Souche, J.-C., 2021. Eco-design of Marine Infrastructures: towards Ecologically-Informed Coastal and Ocean Development. John Wiley & Sons.

Reguero, B.G., Beck, M.W., Agostini, V.N., Kramer, P., Hancock, B., 2018. Coral reefs for coastal protection: a new methodological approach and engineering case study in Grenada. J. Environ. Manag. 210, 146–161. https://doi.org/10.1016/j.jenvman.2018.01.024.

Reguero, B.G., Storlazzi, C.D., Gibbs, A.E., Shope, J.B., Cole, A.D., Cumming, K.A., Beck, M.W., 2021. The value of US coral reefs for flood risk reduction. Nat. Sustain. 4, 688–698. https://doi.org/10.1038/s41893-021-00706-6.

Reidenbach, M.A., Stocking, J.B., Szczyrba, L., Wendelken, C., 2021. Hydrodynamic interactions with coral topography and its impact on larval settlement. Coral Reefs 40, 505–519. https://doi.org/10.1007/s00338-021-02069-y.

Rhode-Barbarigos, L., 2022. SEAHIVE - Sustainable Estuarine and Marine Revetment (No. 213), NCHRP IDEA Project. National Academies.

Rogers, J.S., Monismith, S.G., Feddersen, F., Storlazzi, C.D., 2013. Hydrodynamics of spur and groove formations on a coral reef. J. Geophys. Res.: Oceans 118, 3059–3073. https://doi.org/10.1002/jgrc.20225.

Rogers, J.S., Monismith, S.G., Koweek, D.A., Dunbar, 2015. Wave dynamics of a Pacific Atoll with high frictional effects. J. Geophys. Res. : Oceans 121, 350–367. https://doi.org/10.1002/2015JC011170.

Seelig, W., 1980. Two-Dimensional Tests of Wave Transmission and Reflection Characteristics of Laboratory Breakwaters. Coastal Engineering Research Center.

Sharifahmadian, A., 2015. Numerical Models for Submerged Breakwaters: Coastal Hydrodynamics and Morphodynamics. Butterworth-Heinemann.

Sheppard, C., Dixon, D.J., Gourlay, M., Sheppard, A., Payet, R., 2005. Coral mortality increases wave energy reaching shores protected by reef flats: examples from the Seychelles. Estuar. Coast Shelf Sci. 64, 223–234. https://doi.org/10.1016/j.ecss.2005.02.016.

Stocking, J.B., Rippe, J.P., Reidenbach, M.A., 2016. Structure and dynamics of turbulent boundary layer flow over healthy and algae-covered corals. Coral Reefs. https://doi.org/10.1007/s00338-016-1446-8.

Storlazzi, C.D., Reguero, B.G., Alkins, K.C., Shope, J.B., Gaido-Lassarre, C., Viehman, T.S., Beck, M.W., 2025. Hybrid coral reef restoration can be a cost-effective nature-based solution to provide protection to vulnerable coastal populations. Sci. Adv. 11, eadn4004. https://doi.org/10.1126/sciadv.adn4004.

Tomasicchio, G.R., D'Alessandro, F., 2013. Wave energy transmission through and over low crested breakwaters. J. Coast Res. 398–403. https://doi.org/10.2112/SI65-068.

USCRTF, 2020. Coral reefs as national natural infrastructure. U.S. Coral Reefs Task Force Resolution 47 (2).

van den Brekel, E., 2021. Hydrodynamic and Ecological Performance of a New Modular Unit for Living Breakwaters: Wave Flume Experiments and Results (Masters Thesis). TU Delft.

van der Meer, J.W., Pilarczyk, K.W., 1990. Stability of low crested and reef breakwaters. Coastal Engineering Proceedings. https://doi.org/10.9753/icce.v22.

van Gent, M.R.A., Buis, L., van den Bos, J.P., Wüthrich, D., 2023. Wave transmission at submerged coastal structures and artificial reefs. Coast. Eng. 184, 104344. https://doi.org/10.1016/j.coastaleng.2023.104344.

Viehman, T.S., Reguero, B.G., Lenihan, H.S., Rosman, J.H., Storlazzi, C.D., Goergen, E.A., Canals Silander, M.F., Groves, S.H., Holstein, D.M., Bruckner, A.W., Carrick, J.V., Haus, B.K., Royster, J.B., Duvall, M.S., Torres, W.I., Hench, J.L., 2023. Coral restoration for coastal resilience: integrating ecology, hydrodynamics, and engineering at multiple scales. Ecosphere 14, e4517. https://doi.org/10.1002/ecs2.4517.

Vijay, K., Neelamani, S., Nishad, C., Sahoo, T., 2021. Gravity wave interaction with multiple submerged artificial reefs. Proc. IME M J. Eng. Marit. Environ. 235, 607–622. https://doi.org/10.1177/1475090220960848.

Vitousek, S., Barnard, P.L., Fletcher, C.H., Frazer, N., Erikson, L., Storlazzi, C.D., 2017. Doubling of coastal flooding frequency within decades due to sea-level rise. Sci. Rep. 7, 1–9. https://doi.org/10.1038/s41598-017-01362-7.

von Schnering, H.G., Nesper, R., 1991. Nodal surfaces of Fourier series: Fundamental invariants of structured matter. Z. Physik B - Condensed Matter 83, 407–412. https://doi.org/10.1007/BF01313411.

Vyzikas, T., Stagonas, D., Buldakov, E., Greaves, D., 2018. The evolution of free and bound waves during dispersive focusing in a numerical and physical flume. Coast. Eng. 132, 95–109. https://doi.org/10.1016/j.coastaleng.2017.11.003.

Wilcox, D.C., 2006. Turbulence Modeling for CFD. DCW Industries. Inc, La Canada, CA.

Woo, J., Kim, D., Yoon, H.-S., Na, W.-B., 2014. Characterizing Korean general artificial reefs by drag coefficients. Ocean Engineering 82, 105–114. https://doi.org/10.1016/j.oceaneng.2014.02.025.